Low-Frequency Modes of Vorticity and Divergence in Monsoon Intraseasonal Oscillation

Rajat Masiwal[1], Ashwin K Seshadri[1,2]

[1] Centre for Atmospheric and Oceanic Sciences, Indian Institute of Science, Bengaluru, India.

[2] Divecha Centre for Climate Change, Indian Institute of Science, Bengaluru, India.

Corresponding author: Rajat Masiwal (rajatmasiwal@iisc.ac.in)

Key Points:

- Northward propagating low-frequency oscillatory modes are present in vorticity and divergence during monsoon.
- Oscillatory mode of vorticity has equivalent barotropic structure while divergence has baroclinic vertical structure.
- Rainfall is in phase with the baroclinic divergence but lags barotropic vorticity near equator and leads it away from the equator.

Abstract

The low-frequency intraseasonal oscillations (ISOs) dominate the subseasonal variability of the Indian summer monsoon and involve rainbands propagating northward from the equator. These oscillations modulate the active–break cycle of the monsoons and have two distinct regimes, one where rainfall maximum is located near the equator and the second one in which it is located around central India. The interaction of vorticity and divergence is an important feature for the northward propagation of ISOs. With a correlation study, we show that the low-frequency modes in vorticity and divergence are coupled in the boundary layer and upper troposphere. We use multichannel singular spectrum analysis to extract the low-frequency oscillatory modes in vorticity and divergence. The examination of the spatiotemporal structure of these modes reveals that vorticity has coherent northward propagation at all pressure levels. In contrast, divergence only shows propagation in the boundary layer and the upper troposphere. The vorticity low-frequency mode has a near barotropic structure, while the divergence mode has a baroclinic structure. We point out the contrasting features of vorticity and divergence for the two regimes of the ISO. The barotropic vorticity leads the rainfall for the equatorial region, whereas, for the central Indian region, the vorticity lags the rainfall. Meanwhile, the rainfall is in phase with baroclinic divergence for both regimes. These findings are relevant to understanding the initiation and propagation of ISOs and can contribute to the further development of simple models of these phenomena.

Introduction

The Indian summer monsoon is a complex system involving variability at various spatial and temporal scales. Monsoon intraseasonal oscillation is one of the key recurring features of the Indian summer monsoon, dominating its subseasonal variability. These oscillations are usually divided into two categories depending upon the period, the 10-20 days high-frequency oscillations and 20-60 days low-frequency oscillations. The low-frequency intraseasonal oscillations (ISOs) have an associated northward propagation of cloud bands from the equator to the Indian land region until 30°N (Yasunari, 1979) and can explain 17-40% of the total monsoon rainfall variance (Karmakar et al., 2017). This northward propagation is linked to the maximum cloud zone (MCZ) migrating northward (Sikka & Gadgil, 1980). The active and break spells with enhanced and suppressed rainfall respectively in the core monsoon zone are modulated by the phases of these ISOs. Gadgil (1995) pointed out that longer breaks during monsoon season can adversely affect agricultural production. This suggests that the understanding of ISOs is essential for the subseasonal forecasting and managing agricultural production.

Many studies have offered accounts of the spatial and temporal evolution of various fields during ISO with the help of a data-driven filtering method called the multichannel singular spectrum analysis (MSSA). MSSA can be used to extract the spatiotemporal patterns from a multivariate timeseries. Unlike linear filters, which make use of predefined basis function and bandwidth, MSSA uses the input data to identify the choice of basis and is able to extract nonlinear oscillations. Krishnamurthy & Shukla (2007) used MSSA on a gridded rainfall dataset and showed that the 45-days intraseasonal mode propagates northward. Krishnamurthy & Achuthavarier (2012) used the same method on the horizontal and vertical winds and found that the northward propagating mode is present in the wind fields with a local Hadley cell moving northward. Hazra & Krishnamurthy (2015), after estimating the diabatic

heating from the residual of the thermodynamic equation, performed MSSA on the values of this heating and extracted a 45 day northward propagating intraseasonal mode having its maximum amplitude in the middle troposphere. More recently, Karmakar et al. (2017) used MSSA on satellite-based rainfall observations to identify and extract the 10-20 days and 20-60 days intraseasonal oscillations, with the latter showing northward propagation. Their study also showed that the intensity of the 20-60 day oscillatory mode negatively correlates with all Indian monsoon rainfall.

Based on dynamics and thermodynamics, various mechanisms have been suggested for the northward propagation of low-frequency ISOs. Jiang et al. (2004) used a linear 2.5-layer model to show that the northward propagations result from the interaction of barotropic and baroclinic modes in the presence of mean easterly wind shear. The study suggested that the baroclinic divergence in the presence of mean easterly shear gives rise to barotropic vorticity to the north of previous convection, which then causes the generation of barotropic divergence, which then results in the boundary layer convergence to move northward of the previous convection. This mechanism was also supported by a separate modeling study by Drbohlav & Wang (2005). DeMott et al. (2013) compared the different mechanisms of northward propagation and concluded that the advection of boundary layer moisture and barotropic vorticity generation are the most important processes. The model of Jiang, although qualitatively correct, made use of unrealistic values of the diffusion and friction coefficient (Bellon & Srinivasan, 2006). Dixit & Srinivasan (2011) modified the Jiang model by incorporating a mean meridional shear resulting in better scale selection with more realistic values for diffusion coefficient. Using a coupled climate model Y. M. Yang et al. (2019) showed that the Tibetan Plateau plays an important role in creating the observed shear in zonal winds. Removal of the Tibetan Plateau from the model produces a decrease in the generation of barotropic vorticity, ultimately weakening the northward propagations of ISOs. Yang et al. (2019) simulated the northward propagating signal in an intermediate complexity model with multicloud parametrization and noted the absence of barotropic divergence during the northward propagating intraseasonal event in their model. Recently, Li et al. (2021) suggested that it is the vorticity tilting term that causes the generation of positive vorticity to the north of convection and that the structure of this tilting term is not captured well in climate models. The importance of the tilting term was also pointed out in an earlier study by Yokoi & Satomura (2006). All these studies suggest that vorticity and divergence play a key role in the northward propagation mechanism of LF-ISOs.

There have been several studies reporting the vertical structure of vorticity and divergence with respect to the location of maximum convection in the LF-ISO mode (Jiang et al. (2004); Abhik et al. (2013); Zheng & Huang (2019)). All these studies report that a near barotropic vorticity structure appears to the north of convection center. They also show that divergence has a baroclinic structure, with boundary layer convergence being at the convection center or slightly to the north and upper-level divergence being a few degrees south of the convection center. These studies are based on making composites of the fields about the convection maximum, irrespective of that maximum being near equator or away from it. A detailed description of the structure of these fields for the two different regimes of rainfall during ISO is still missing.

This study aims to document the space-time structure of vorticity and divergence and the associated northward propagation of these variables during the intraseasonal oscillation in

the Indian monsoon domain. We use ERA5 reanalysis to perform a correlation study to understand the coupling of vorticity and divergence at different pressure levels. We extract the low-frequency intraseasonal modes in both these variables using multichannel singular spectrum analysis (MSSA). Resulting phase composites of these modes are analyzed to reveal the horizontal and vertical structures of vorticity and divergence during the monsoon intraseasonal oscillation. We note the similarities and differences in these structures for the two regimes of the rainfall ISO, one being when the rainfall maximum is near the equator and the other one when the rainfall maximum is around 20°N. The rest of the paper is organized as follows. Section 2 describes the dataset used and the method of analysis for this study. Section 3 describes the main results of the study. Finally, we present the conclusion and a brief discussion in section 4.

2. Data and methods

2.1 Data

In this study, we have used Tropical Rainfall Measuring Mission (TRMM) 3B42 (V7) daily rainfall data for 1998-2018 (Huffman et al., 2007). To help reduce the computational cost, the data is regridded to 1° × 1° resolution using bilinear interpolation.

We have also used daily instantaneous values of vorticity, divergence, and horizontal winds from ERA5 reanalysis (Hersbach et al., 2020) at 17 different pressure levels from 1000hPa to 200hPa at an interval of 50hPa. For consistency, the horizontal resolution of ERA5 variables is also 1° × 1° and the analysis is done for the same time-period as the rainfall data (1998-2018). Since we examine the intraseasonal oscillations occurring in the South Asian monsoon region, our domain of analysis is restricted to 10°S-35°N and 60°E-110°E.

2.2 Methods of analysis

a) Multichannel Singular Spectrum Analysis (MSSA)

For extracting the intraseasonal modes in rainfall, vorticity, and divergence, we have performed multichannel singular spectrum analysis (MSSA) on all the three fields separately. MSSA is a data-adaptive filtering technique that can separate various oscillatory components and trends present in the data. It involves constructing a trajectory matrix T by taking M lagged copies of a multivariate time-series of length N and having L channels (or grid points) and then constructing a lagged covariance matrix C with lags ranging from 0 to $M-1$. Upon diagonalization of the covariance matrix (C) of Trajectory matrix (T), one obtains LM eigenvalues and LM eigenvectors. These eigenvectors are also called space-time empirical orthogonal functions (ST-EOFs). The corresponding space-time principal components (ST-PCs) are obtained by projecting the data from the trajectory matrix T onto each of the LM eigenvectors. The respective eigenvectors and PCs are then combined to obtain reconstructed components (RCs) which have the same length as the data. These RCs contain the various modes present in the original data. Comprehensive details of MSSA and its foundations can be found in the review by Ghil et al. (2002).

Our implementation of MSSA for extracting oscillatory modes in rainfall is similar to that used by Krishnamurthy & Shukla (2007). We first compute the daily anomaly of rainfall by removing the daily climatology (for the period 1998-2018) from the original rainfall data. The anomaly data is then smoothened by estimating a five-day running mean, and then data

from June to October (122 days) for the whole period of analysis is fed to the MSSA algorithm. The low-frequency mode that we recover from the various reconstructed components obtained using the MSSA procedure is then used for further analysis.

For the 4-D vorticity and divergence variables, an approach similar to Krishnamurthy & Achuthavarier (2012) is used where we first compute the anomaly by removing the daily climatology and then the data at each vertical level is normalized by its respective root mean square value so that variance in the MSSA modes is not dominated by any one particular vertical level. After this, we perform an EOF analysis on the data and take the first 1000 principal components, which explain around 95% of the variance in the original data, as the channels for MSSA. This helps in reducing the computational cost.

b) Phase Composites

To analyze the intraseasonal modes recovered with the help of MSSA, we compute the phase angles and amplitude of the oscillatory mode present in rainfall using the method given in Moron et al. (1998). The phase angle is computed for each day and lies between $-\pi$ to π for the entire period of analysis. To understand the evolution of different fields during the oscillation, the entire period is divided into different phases. All the days for which the angle falls in a particular phase are averaged to get composite maps for that phase. The evolution of these phase composites helps us understand the overall behavior of various fields during intraseasonal oscillations.

3. Results

3.1 Mean structure of Vorticity and Divergence

To understand how vorticity and divergence evolve during the monsoon months, we examine the June-September (JJAS) mean of daily climatology (from 1998-2018) for each of these fields. The latitude-pressure sections of vorticity and divergence, also in addition to spatially averaged rainfall between 70E-90E are shown in Fig. 1. There is positive vorticity away from the equator in the summer hemisphere and the maximum of vorticity is above the boundary layer at about 850hPa. As for divergence, while there is convergence throughout the Indian land region, large values of convergence as well as maximum convergence are confined to the lower troposphere near the boundary layer; while at the top of the troposphere, we see strong divergence for the whole domain. The daily standard deviation (Figure S1.) for both vorticity and divergence are high in the summer hemisphere suggesting that for the Indian monsoon region, there is a substantial variation in these fields at the intraseasonal timescale. The daily mean rainfall climatology shows two maxima (Fig. 1), one slightly south of the equator and one close to 20°N. For the maxima at 20°N, there is strong convergence in the boundary layer and cyclonic vorticity, and for the maxima slightly south of the equator, we again find cyclonic vorticity now in the southern hemisphere along with boundary layer convergence.

Now to study the intraseasonal variation of vorticity and divergence, we first take the help of conventional bandpass filtering. Both these fields are 20-60 days bandpass filtered using the Butterworth filter for the entire analysis period, as we are only focused on the low-frequency component of the monsoon intraseasonal oscillation. The time-latitude plot of filtered fields at 900hPa pressure level suggests the presence of strong intraseasonal activity of

20-60 day period for both vorticity and divergence during the monsoon months. These oscillations are accompanied by northward propagation during these months, which is a signature of low-frequency intraseasonal oscillations (Figure S2.). The meridional structure of vorticity and divergence at 900hPa seem to align during the monsoon period. To investigate if vorticity and divergence are aligned through the depth of the troposphere, the daily correlation between the meridional cross-sections of vorticity and divergence was computed throughout the year for the entire analysis period and all the pressure levels. Fig. 2 shows the distribution of the total number of days in each month of the year for the 21-year period, during which the correlation coefficient between the meridional structure of vorticity and divergence exceeds the value of 0.5 in magnitude and is significant (at 5% significance level). In the boundary layer, the vorticity and divergence are negatively correlated during the monsoon months. With increasing height, this association starts to disappear and is barely present in the lower to middle troposphere. However, in the upper troposphere, we see the situation reversing, and during the monsoon months, there appears a positive correlation between vorticity and divergence. This suggests that, on the intraseasonal timescale, the sign of one of the two fields reverses in the upper troposphere as compared to the boundary layer.

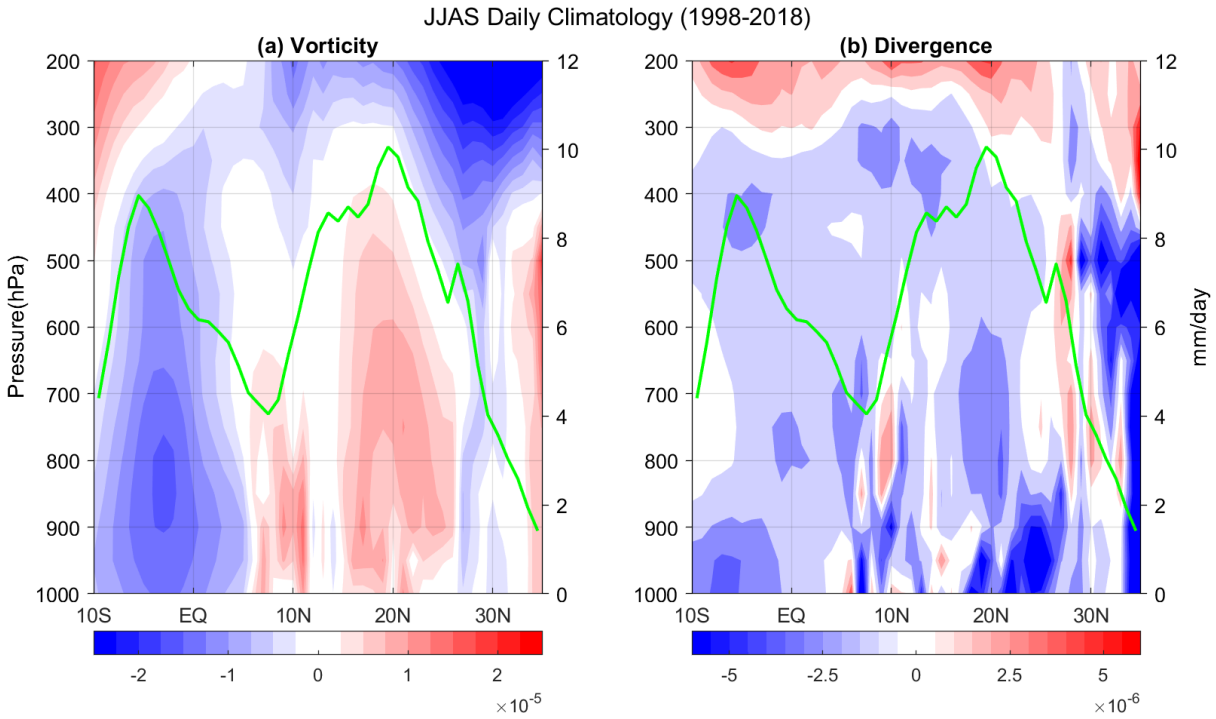

Fig. 1 Latitude-pressure section for mean JJAS daily climatology for (a) vorticity and (b) divergence averaged between 70E-90E. Latitudinal variation of seasonal mean daily rainfall climatology is also plotted (green curve). The units of vorticity and divergence is in s^{-1}

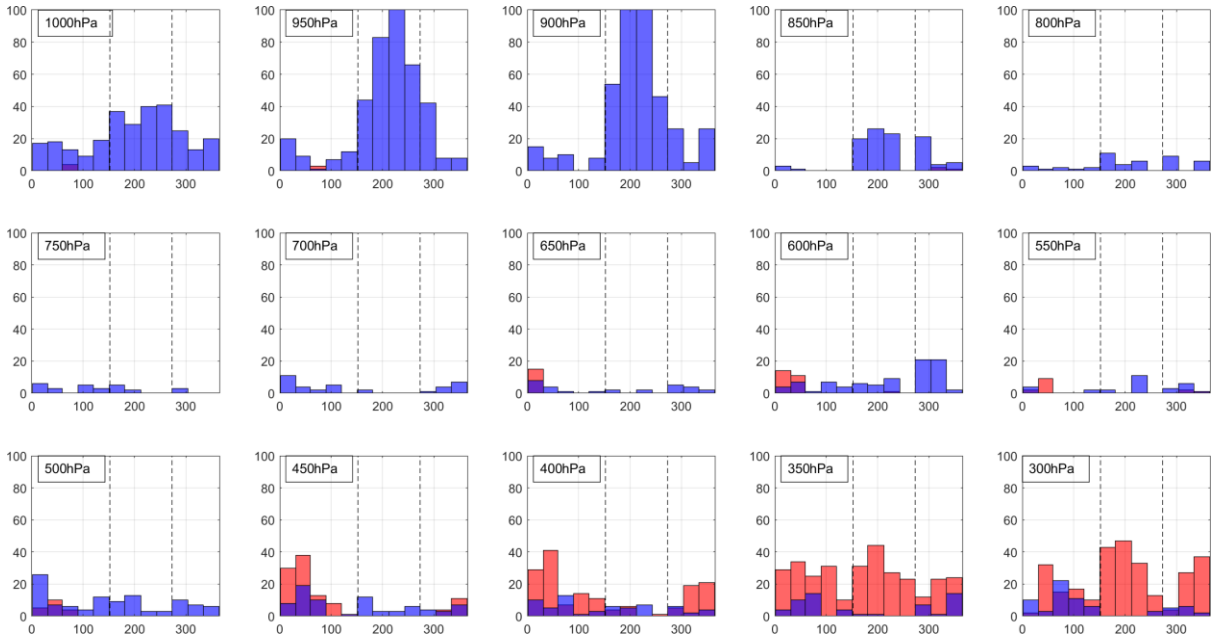

Fig. 2 Number of days in a month of the year for 21 years in which the correlation between the meridional structure of 20-60 days bandpass filtered vorticity and divergence was greater than 0.5 (red) or less than -0.5 (blue). The vertical dotted lines indicate monsoon months. Only days with correlation significant at 5% level are considered.

3.2 Intraseasonal modes through MSSA

To study the vertical structure of vorticity and divergence during the low-frequency intraseasonal oscillation, we apply the technique of MSSA. Firstly, the intraseasonal mode in rainfall was extracted using the same method. Upon applying MSSA on June to September TRMM rainfall data for 1998-2018, it was noted that the first two eigenvalues were similar in magnitude, and the corresponding ST-EOF and ST-PC were in phase quadrature and had similar time-period, thus satisfying the criteria of constituting an oscillatory mode (Plaut & Vautard, 1994). The RCs obtained from these two modes are combined and henceforth referred to as RC (1,2). The power spectra of the principal component corresponding to RC(1,2) show a peak at 40 days, corresponding to the low-frequency mode of intraseasonal oscillation. Moreover, they have a broadband structure, pointing towards the nonlinear nature of the oscillation. Throughout this paper, this reconstructed component will be referred to as rainfall LF-ISO as it represents the low-frequency intraseasonal oscillatory part of the signal.

To understand its evolution, this LF-intraseasonal rainfall mode is divided into eight different phases for the full cycle. The phase composites reveal a similar picture as obtained by Karmakar et al. (2017). We see a northwest-southeast tilted rainband that progressively moves northward from the equator (Fig. 3). Along with this northward propagation, there is an eastward-moving signal around the equator. The lower level (850hpa) wind anomalies averaged for each phase are also shown in Fig. 3. The anomalous wind patterns obtained for each phase resembles the circulation pattern discussed by Krishnamurthy & Achuthavarier, (2012), who extracted oscillatory modes in horizontal winds with the help of MSSA. The cyclonic circulation from the Indian ocean propagates northeastward as positive rainfall anomalies enter the Indian landmass from the equator (phase 2 to phase 6). The positive rainfall anomaly in the central Indian region is associated with strong south-westerlies in the Arabian sea near the western ghats. The rainfall LF-ISO, as suggested by earlier studies too, gives the signature of a typical active-break cycle within a monsoon season.

To study how these oscillations are manifested in vorticity and divergence, MSSA was applied to daily anomalies of vorticity and divergence at all 17 levels, for the months of June to September and the entire period of analysis (1998-2018). Again, for both the fields, the first two eigenvalues are closely spaced, with the corresponding eigenvectors being in phase quadrature. Thus, we obtain the intraseasonal oscillatory modes for both vorticity and divergence by combining their respective ST-EOFs and ST-PCs. The reconstructed components of these fields, similar to rainfall LF-ISO, show broadband type spectra with their corresponding peaks close to 40 days. The present study considers only the low-frequency intraseasonal oscillation, corresponding to a pair of eigenvectors in phase quadrature. Small eigenvalues for both the variables also show other different modes including the high-frequency intraseasonal oscillations, seasonally persisting components, as well as trends during the period of study. These are beyond our present scope. Similarly to rainfall, the reconstructed components of vorticity and divergence are referred to as vorticity LF-ISO and divergence LF-ISO respectively and the first principal components of these ISOs have similar power spectra. (Figure S3.)

Phase composites of vorticity LF-ISO and divergence LF-ISO were generated using the phases of rainfall. Our focus is specifically on the meridional propagations of these ISOs and, to capture these propagations better, the rainfall ISO was divided into 24 phases of equal interval $\pi/12$, and then the vorticity and divergence ISOs were averaged within the different phases. These composites give an indication of time-evolution for these oscillations. Fig. 4 shows the phase-latitude variations of vorticity and divergence LF-ISOs for different pressure levels superimposed along with the rainfall LF-ISO shown in contour lines. The vorticity field shows coherent northward propagation for all the pressure levels and appears to be in phase with the rainfall LF-ISO. In contrast for divergence, the northward propagation is much less coherent and more disaggregated, especially in the lower and middle troposphere. A similar propagation structure for 30-60 days band-pass filtered anomalies of 925hPa divergence and 850hPa vorticity was reported in Goswami (2005). In the upper troposphere, the divergence also shows propagation from the equator to about 25°N. Moreover, rainfall is out of phase with lower-level divergence and in phase with the upper-level divergence. This suggests that the low frequency intraseasonal oscillations are accompanied by lower-level convergence and upper-level divergence.

The horizontal structure of vorticity and divergence LF-ISOs for three different vertical levels (850hPa, 500hPa and 250hPa) are shown in Fig. 5. Maps for phases 3-6 are shown as these four phases represent the half-cycle containing the initiation and propagation of positive rainfall anomaly onto central India, while the other four phases represent the other half of the cycle (Fig. 3). Vorticity ISO at phase 3, for all the three levels, has a positive anomaly at the southern tip of India and flows northward, reaching the core monsoon region (central India) by phase 6. The anomalies cover much of the entire longitude range from 60°E to 110°E. In contrast to vorticity, the divergence ISO is less spatially coherent and more disaggregated. In the lower troposphere, at 850hPa, a convergence anomaly propagates northward from the southern tip of India and the Western Ghats in phase 3 to central India in phase 6. This propagation is not visible at 500hPa and furthermore the magnitude of divergence is low at this pressure level. At 250hPa, there is again a northward propagating signal, but the sign of the divergence is reversed with positive anomalies moving northward towards central India going

from phase 3 to phase 6. All these observations concur well with the latitude-phase plots discussed above. (Fig. 4).

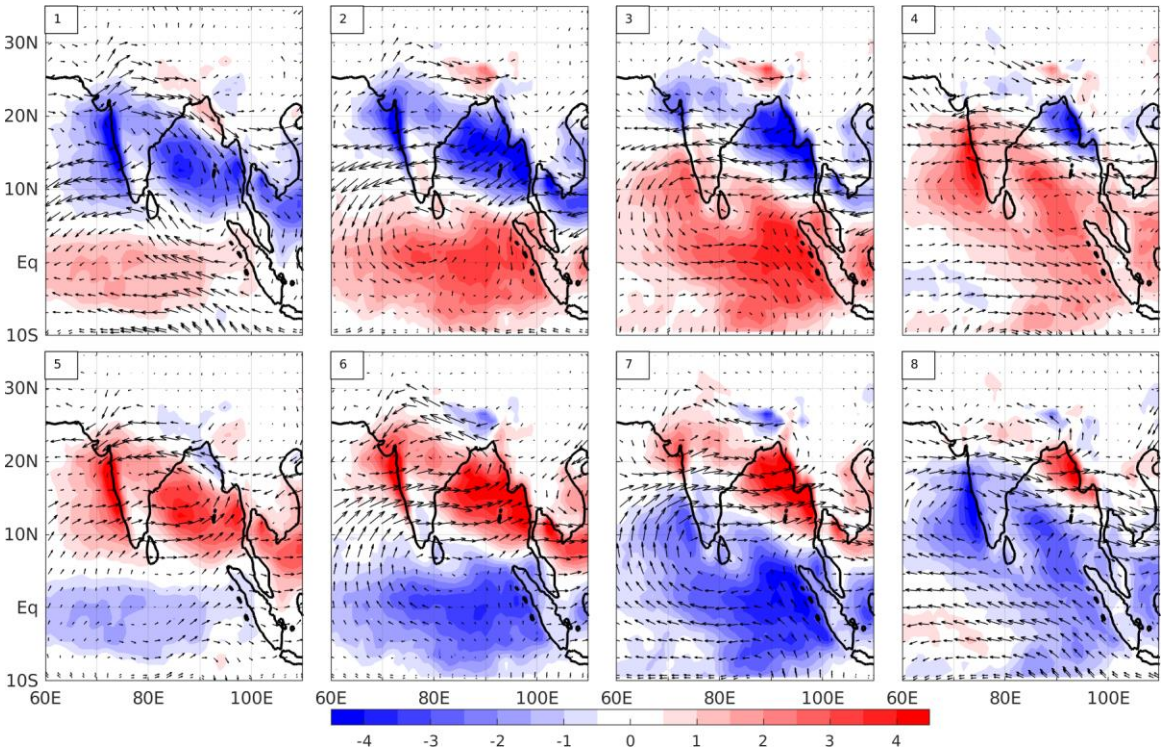

Fig. 3 Phase composites of rainfall low-frequency (LF) ISO in color shading (mm/day) and wind anomalies at 850hPa averaged over the respective phases for the period of 1998 – 2018. The phase number are indicated at the top left.

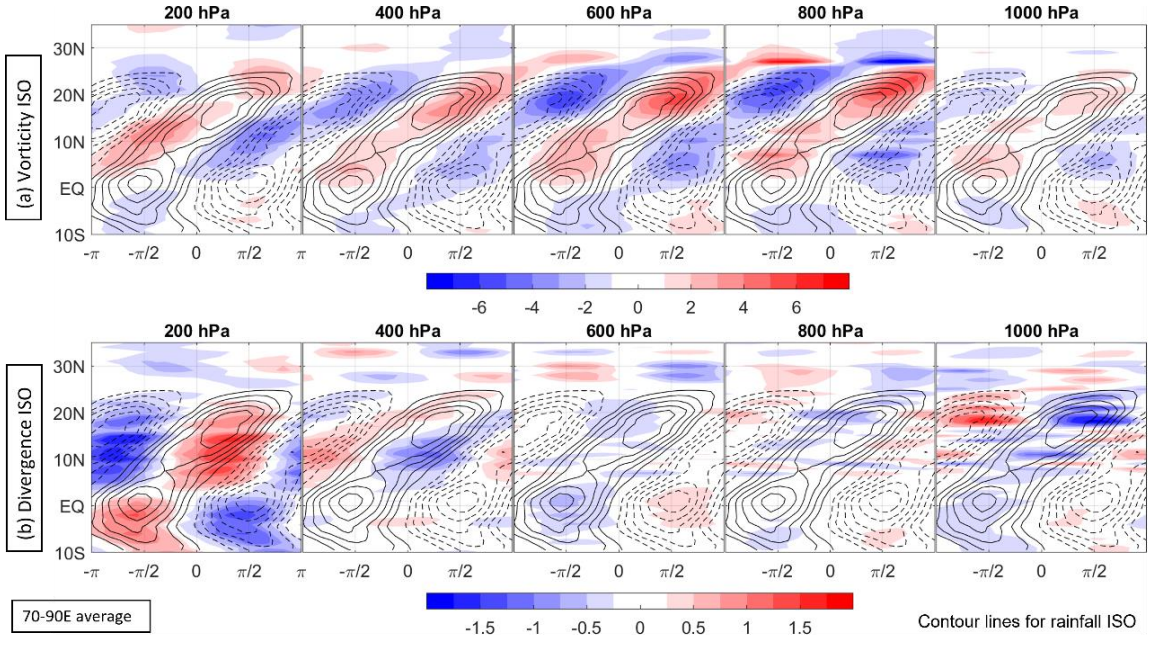

Fig. 4 Latitude - phase section for (a) vorticity and (b) divergence in s^{-1} along with rainfall ISO (dotted contour lines for negative rainfall and solid lines for positive rainfall) for 1998-2018 for different pressure levels indicated at the top of each panel.

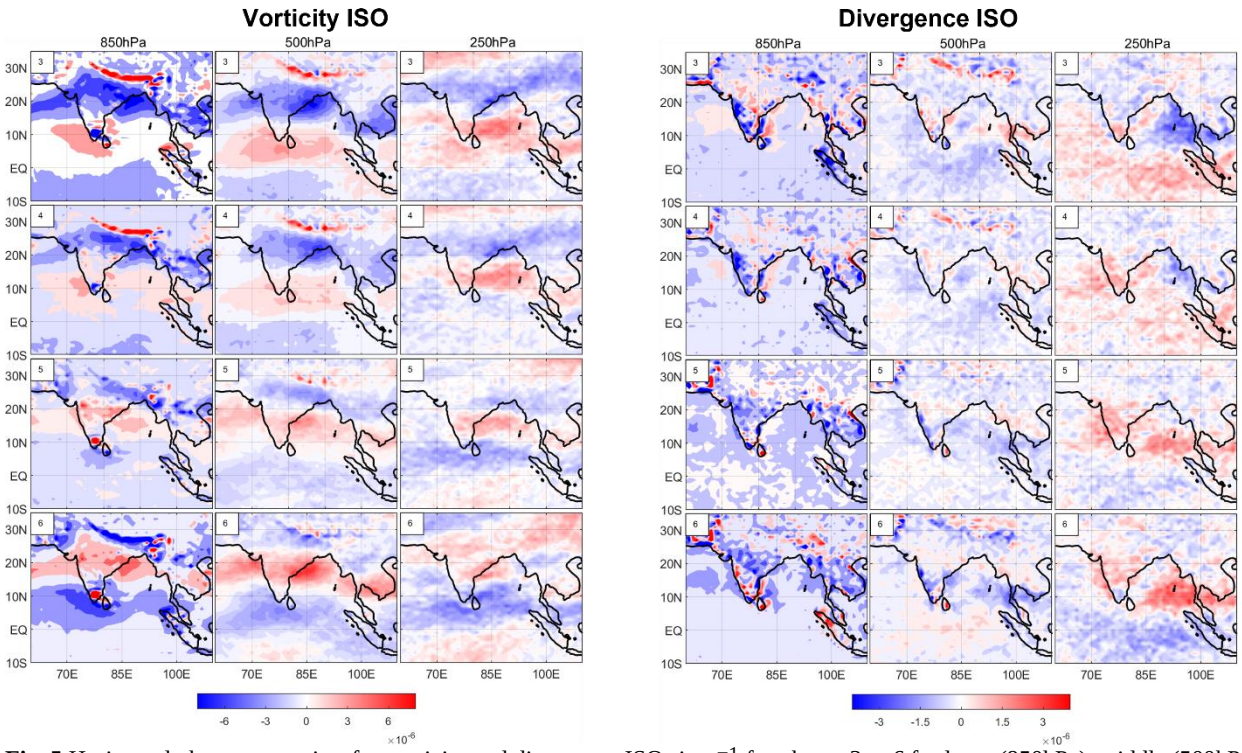

291 **Fig. 5** Horizontal phase composites for vorticity and divergence ISOs in s^{-1} for phases 3 to 6 for lower(850hPa), middle (500hPa) and upper (250hPa) troposphere. The phases are based on rainfall ISO from Fig. 3.

292 ### 3.3 Vertical structure of low-frequency oscillations in vorticity and divergence

293 Fig. 6 shows the vertical cross-sections of phase composites for vorticity LF-ISO,
294 obtained by averaging from 70°E - 90°E. Also shown are the meridional profiles of rainfall
295 LF-ISO averaged over the same longitude range. A positive vorticity anomaly appears close to
296 the equator in phase 1. This anomaly strengthens, covering the entire depth of troposphere and
297 moves northward in phase 2, with the maximum in rainfall anomaly being located a few degrees
298 south of the vorticity maximum. This positive anomaly of vorticity continues to propagate
299 northward in phases 3 and 4, reaching 15°N at the end of phase 4. The signal strengthens even
300 more along with the increase in the rainfall anomaly in phases 5 and 6, with rainfall maxima
301 reaching 20°N. Simultaneously, negative vorticity covers the equator accompanied by negative
302 rainfall anomaly in this region. The positive vorticity anomaly reaches 25°N by phase 8 with
303 the weakening of rainfall as the cycle nears its completion. The vertical structure is somewhat
304 different for the two main regimes of these oscillations, one where the maximum rainfall
305 anomaly is near the equator (0-10N) and the other when the maximum is located at 15N-20N.
306 During the first regime (break phase of rainfall over central India), the vorticity has multiple
307 local maxima in the vertical, with the vorticity maximum located few degrees to the north of
308 rainfall maxima. Whereas, for the second regime (active phase over central India), the vorticity
309 has a single maximum at around 750hPa and a distinct southward tilt with increasing height in
310 the troposphere. The vorticity in the lower troposphere leads the rainfall maxima by few
311 degrees, while for the middle and upper troposphere it is collocated with rainfall in view of the
312 tilted structure. Moreover, the overall picture suggests vorticity during a low-frequency
313 intraseasonal oscillation having an equivalent barotropic structure with this effect being more
314 predominant away from the equator. This has been explored further in the next section.

315 Fig. 7 shows the vertical structure for phase composites of the divergence LF-ISO.
316 While it has a less evident northward propagating structure as compared to vorticity, the
317 convergence in the lower troposphere moves northward from the equator in phase 1 to 25°N
318 by phase 8. For phase 6 and 7, there is almost a standing pattern at 25°N for boundary layer
319 convergence accompanied by rainfall. Moreover, the divergence LF-ISO has opposite signs in
320 lower and upper troposphere during all the phases of oscillation: pointing towards the
321 substantially baroclinic structure of divergence in the LF-ISO. Again, for the two different
322 regimes noted above, there exist differing structures of the divergence field. During the phase
323 of high near-equatorial precipitation (0-10N), the divergence anomalies are weaker in the
324 boundary layer and stronger in the middle of the troposphere. In contrast, during the phase of
325 high off-equatorial precipitation (15N-25 N), convergence is high in the boundary layer, while
326 the middle troposphere has very small values of either convergence or divergence. Generally,
327 in both regimes, the latitude of convergence maximum coincides with or is slightly to the north
328 of the latitude of maximum precipitation. Furthermore, in the second regime with strong
329 boundary layer convergence, the maximum in the upper tropospheric divergence appears
330 southward of maximum convergence. This tilt between the lower level convergence and upper
331 level divergence was also reported in Yokoi & Satomura (2006) for the Bay of Bengal region.

332 The vertical structure of LF-ISO vorticity and divergence obtained for phase 6 of the
333 oscillation, when the rainfall maximum is in central India, resembles that reported in Abhik et
334 al. (2013) where they plotted the meridional-vertical section composite of anomalous vorticity
335 and divergence relative to the maximum convergence zone.

336 We previously discussed two distinct regimes in rainfall maxima, having different
337 vertical structures of vorticity and divergence. These are examined further in Fig. 8 which
338 shows the vertical variation of LF-ISO vorticity and divergence for the two different regimes.
339 The upper panel show pressure-phase cross-section for the off-equatorial region, 70°E-90°E
340 and 15°N-25°N, for both vorticity and divergence. Vorticity shows a standing pattern that is
341 nearly barotropic with a single maximum at around 750hPa. In this region, the rainfall leads
342 the vorticity by 3-4 days. Large negative values of divergence in the boundary layer, that is
343 convergence, is accompanied by large positive divergence in the upper troposphere, with small
344 values in the middle. Here the divergence and rainfall are in phase with zero or very small lags.
345 The bottom panels in Fig. 8 show the phase evolution for the near-equatorial regime, averaged
346 over 70°E-90°E and 0-10°N. As mentioned earlier, in this case the vorticity has multiple local
347 maxima, appearing at the lower troposphere, middle, and upper troposphere. As for divergence
348 in the equatorial region, the magnitude of the oscillation is comparatively larger in the mid-
349 troposphere than the boundary layer. Here too, the rainfall is in phase with divergence but
350 slightly lags vorticity.

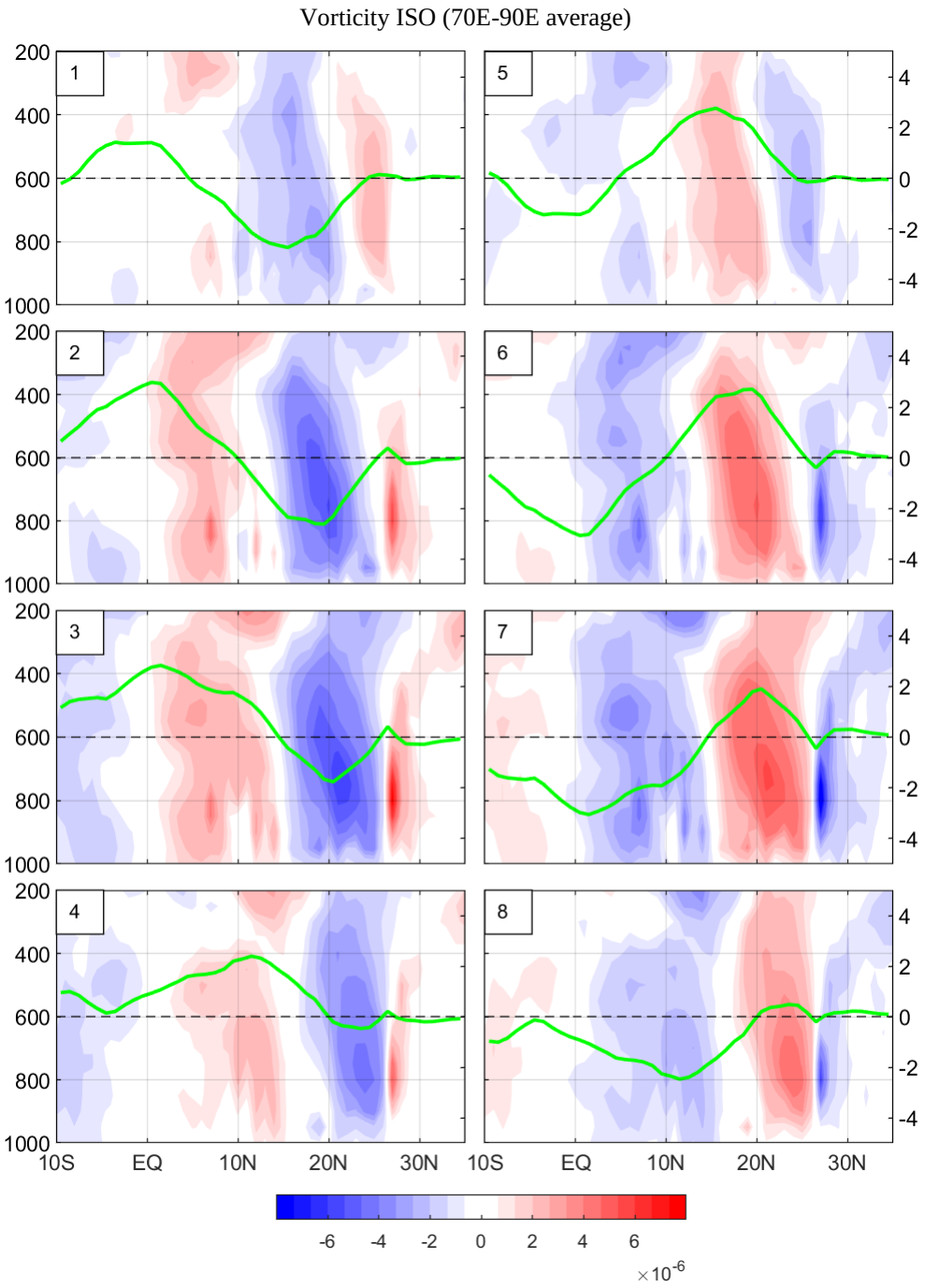

Fig. 6 Pressure-latitude section of phase composite for vorticity LF-ISO (s^{-1}) averaged between 70E-90E. The green curves show the latitudinal variation of rainfall LF-ISO averaged over the same longitudes in mm/day for each phase. The phase number is indicated on the top right of each panel.

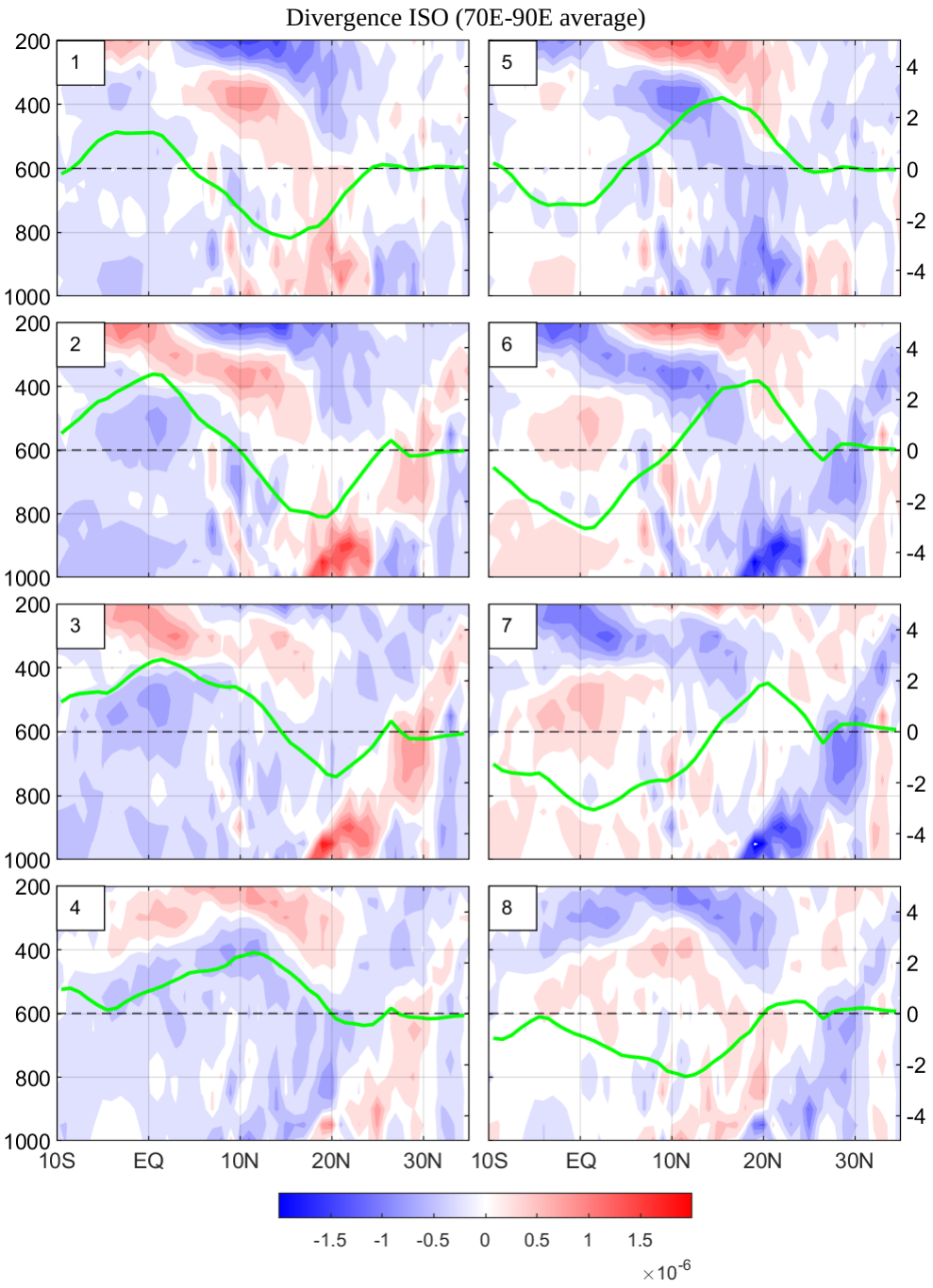

Fig. 7 Pressure-latitude section of phase composite for divergence LF-ISO (s^{-1}) averaged between 70E-90E. The green curves shows the latitudinal variation of rainfall LF-ISO averaged over the same longitudes in mm/day for each phase. The phase number is indicated on the top right of each panel.

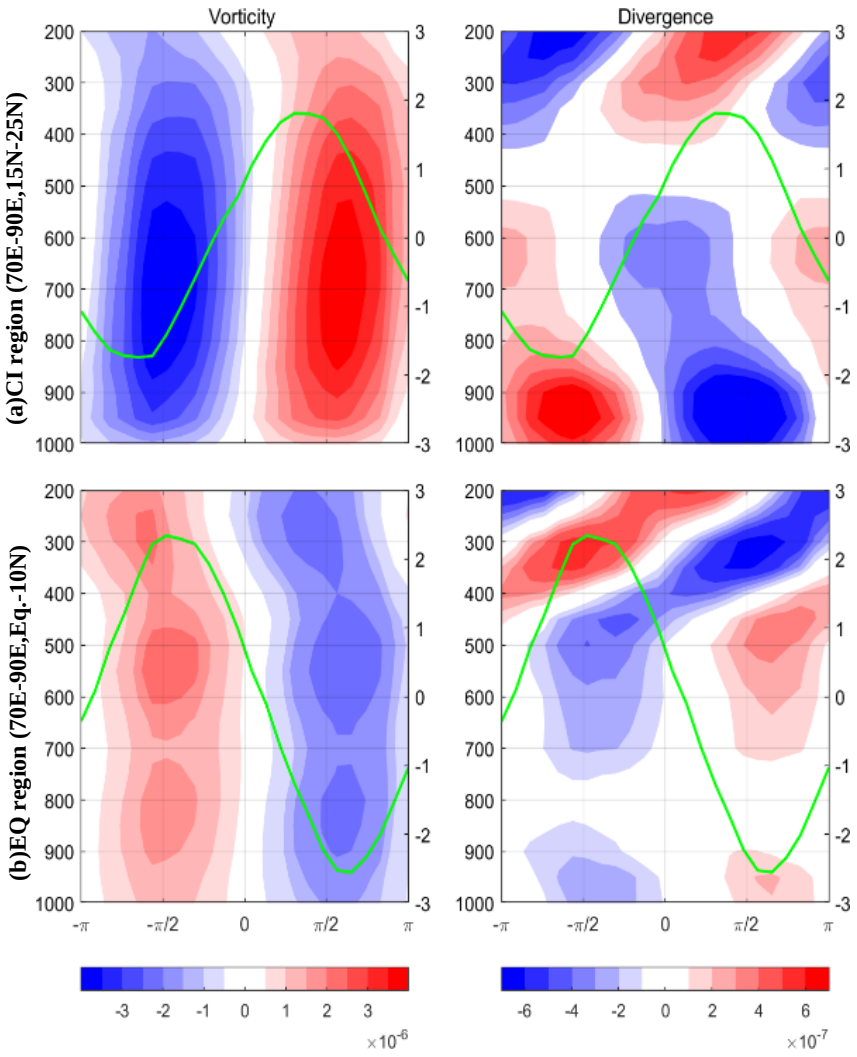

Fig. 8 Pressure-phase section of vorticity and divergence LF-ISO in s^{-1} for (a) central Indian region averaged from 70E - 90E and 15N-25N and (b) equatorial region averaged from 70E-90E and 0 -10N. The green curve shows the phase variation of rainfall LF-ISO for the respective regions in mm/day.

3.4 Barotropic vorticity and baroclinic divergence

The vertical structure of low-frequency vorticity and divergence for both regions of rainfall maxima are examined by performing a principal component analysis (PCA) on the respective regionally averaged time series of the reconstructed components yielded by the MSSA. The vertical modes of vorticity and divergence for the two regions are further decomposed into the vertical eigenvectors (empirical orthogonal functions, "EOFs") obtained from PCA. For the central Indian region (70°E-90°E and 15°N-25°N), the first mode (i.e., the first EOF) in vorticity, shown in Fig. 9a, explains almost all the variance and has a near barotropic structure with a single maximum close to 700hPa. The second mode of vorticity has a baroclinic structure, but its contribution is negligibly small, resulting in an overall barotropic structure of vorticity away from the equator. For divergence, the first mode (the first EOF) has 82% contribution to the variance and is baroclinic with its maximum occurring in the boundary layer. The second mode is also baroclinic, explaining approximately 18% of the variance and having peaks at 600hPa and 300hPa (Fig. 9a). Fig. 9b shows the first two vertical structure modes of vorticity and divergence for the equatorial region (70°E-90°E and 0-10°N). The first mode again appears largely barotropic for vorticity, but in this case having three local maxima

around 800hPa, 550hPa, and 250hPa. The second mode is baroclinic and explains 7% of the variance in the reconstructed component, with higher amplitudes in the upper troposphere. This gives the vorticity a less barotropic structure near the equator. Divergence has a more equal distribution of the contribution from the first two modes with the first one explaining 61.5% and the second mode explaining 38.3% of the variance present in the divergence LF-ISO. The first mode has maxima at 450hPa and 300hPa, whereas the second mode only has significant values at the upper atmosphere and is almost negligible in the lower troposphere. Clearly, the LF-ISOs for both vorticity and divergence have simple vertical structures, with a few modes together constituting much of the variance.

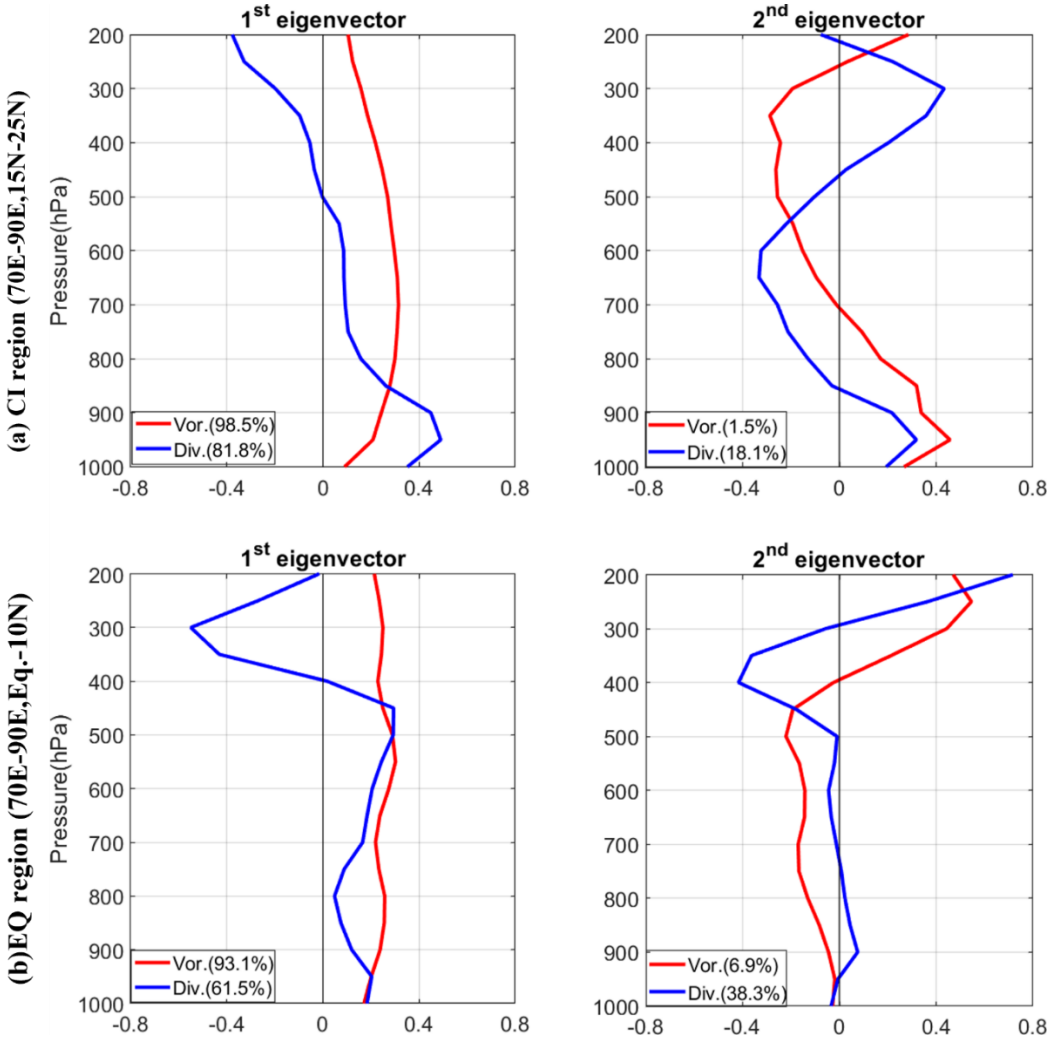

Fig. 9 The vertical structure of first two modes obtained from PCA of vorticity (red) and divergence (blue) LF-ISOs averaged from (a) 70E-90E and 15N-25N and (b) 70E-90E and 0-10N. The percentage variance explained by each mode is written in the box inside each panel.

By projecting both the vorticity and divergence LF-ISO reconstructed components for the entire domain onto the first vertical modes of the central Indian region in Fig. 9a, barotropic vorticity and baroclinic divergence ISOs are estimated. The reason for projecting the entire domain onto the central Indian mode is merely to obtain a spatially continuous map. Our result does not change qualitatively even if we compute EOFs by averaging from 0-14N and 15-30N respectively and then project the reconstructed components for each of these latitude bands onto the respective dominant vertical EOFs of vorticity and divergence (Figure S4.). Both these

variables show a northward propagation and are negatively correlated with each other (Fig. 10). Moreover, for the equatorial region, the barotropic vorticity maximum appears 5° northward of the baroclinic divergence maximum. It is observed that below 10N, the barotropic vorticity leads the baroclinic divergence but northward of 15N, the situation reverses and baroclinic divergence starts leading the barotropic vorticity. These lead-lag becomes clearer when we look at the region averaged time-evolution of these terms.

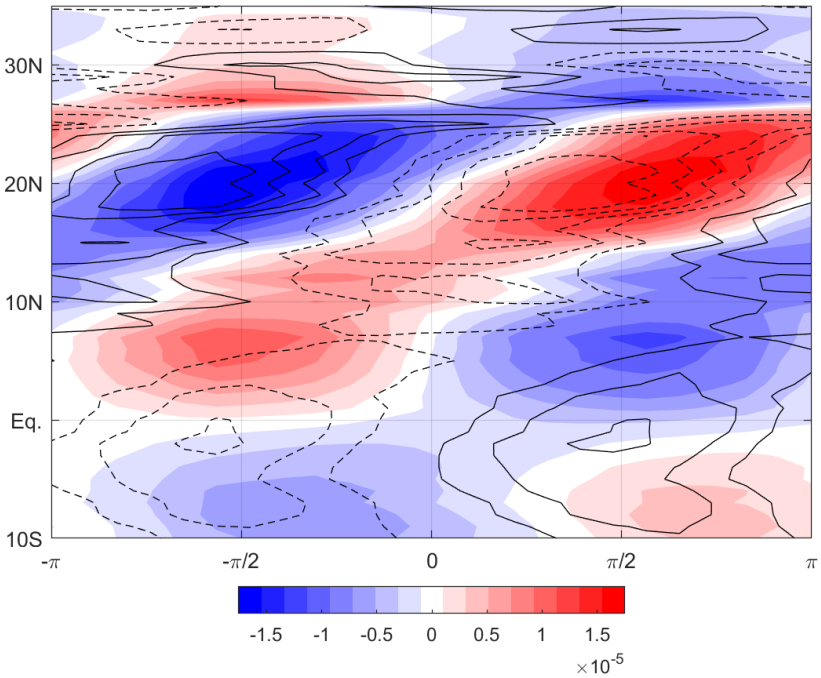

Fig. 10 Latitude-phase section for barotropic vorticity (color shading) and baroclinic divergence (contour line with dotted lines for negative values) in s^{-1} averaged from 70E-90E. The barotropic vorticity and baroclinic divergence are obtained by projecting the vorticity and divergence LF-ISOs onto the first vertical modes given in Fig. 9a

The time-evolution of these projected components, analysed separately for the two regions, reveals the lead-lag relationships between these variables. For the central Indian region, rainfall ISO is in phase with baroclinic divergence ISO but leads barotropic vorticity ISO as can be seen from Fig. 11a. Here, rainfall maximum is achieved around $\frac{\pi}{4}$, along with divergence, whereas the vorticity maximum appears after $\frac{\pi}{2}$. For the equatorial region, vorticity ISO slightly leads the rainfall which is again in phase with divergence ISO. This can be seen in Fig. 11b, where rainfall ISO and baroclinic divergence ISO maxima both appear at $-\frac{\pi}{2}$ with the barotropic vorticity maximum appearing slightly before.

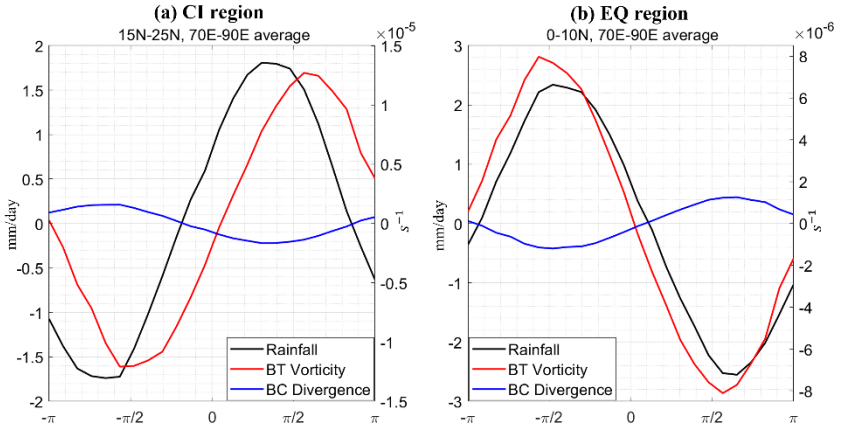

Fig. 11 Phase variation of rainfall LF-ISO (black) in mm/day and barotropic vorticity (red) and baroclinic divergence (blue) in s^{-1} for (a) central Indian region (70E-90,15N-25N average) and (b) equatorial region (70E-90E,0-10N average).The barotropic vorticity and baroclinic divergence are obtained by projecting the three dimensional vorticity and divergence ISO onto the first vertical modes of respective regions given in Fig. 9.

In this study, we examine the spatial and temporal structure of vorticity and divergence during the northward propagating monsoon intraseasonal oscillations. A possible mechanism of northward propagation is linked to the interaction of vorticity and divergence (Jiang et al., 2004), making the study of these two variables extremely relevant in this context. The seasonal mean of daily climatology of vorticity has a positive value in the northern hemisphere along with strong convergence in the boundary layer. This is associated with the shifting of mean intertropical convergence zone (ITCZ) to the north on a seasonal timescale. This ITCZ shift also results in enhanced rainfall in the Indian land region during monsoon months. Both vorticity and divergence fields show considerable variability in the northern hemisphere during the summer monsoon season. We investigate this variability and its connection to the intraseasonal oscillations in rainfall with the help of ERA5 reanalysis and satellite-based rainfall products.

On the 20-60 days timescale, the meridional structure of boundary layer vorticity and divergence is negatively correlated during the monsoon months (JJAS). This correlation is absent for the mid-tropospheric vorticity and divergence. The situation reverses at the top of the troposphere with positively correlated vorticity and divergence during monsoon months. We extract the low-frequency oscillations in both these variables with a data-adaptive filtering technique known as multichannel singular spectrum analysis (MSSA). As in the case of rainfall, the dominant oscillatory mode in both vorticity and divergence, recovered from MSSA, has a dominant time period close to 40 days representing the low-frequency intraseasonal component of monsoon variability. The meridional-phase structure of this low frequency ISO mode of the vorticity field shows a northward propagation from the equator to 25˚N for all pressure levels, with positive vorticity anomalies propagating together with positive anomalies of rainfall LF-ISO. For divergence, the northward propagation is present in the boundary layer and in the upper-troposphere, but these oscillations are much weaker and less coherent in the mid-troposphere.

The positive rainfall LF-ISO propagates with negative divergence (convergence) in the boundary layer, but the situation reverses in the upper troposphere, which has positive divergence associated with positive rainfall anomalies. The vertical structure of the vorticity LF-ISO is nearly barotropic, propagating northward from the equator to central India, with the maximum of vorticity, located around 750hPa, being present a few degrees north of the rainfall maximum. The divergence ISO shows a baroclinic vertical structure with values of opposite signs present in the lower and the upper troposphere. The latitude of rainfall maximum coincides with the maximum in boundary layer convergence, while the upper-level divergence maximum is generally present southward of this latitude.

We quantify the barotropic and baroclinic nature of vorticity and divergence, respectively, through principal component analysis. Away from the equator at 15˚N-25˚N, the barotropic mode of vorticity dominates and explains 98% of the variance and has a maximum around 750hPa while close to the equator (0-10˚N), we also note a baroclinic component of vorticity that plays a somewhat larger role. For divergence, away from the equator the first mode shows a baroclinic structure and explains 82% of the variance in the ISO. Close to the equator, we see the variance is more evenly distributed between the first two baroclinic modes, with the first mode showing 61.5% and the second one showing 38.3% contribution to the divergence ISO. This finding is in line with a recent modeling study by Q. Yang et al. (2019),

which suggested that the equatorial convection results from two competing baroclinic divergence effects.

Projecting the divergence and vorticity LF-ISO onto the first vertical mode, we get the baroclinic divergence and the barotropic vorticity LF-ISO. Since the first modes in each case constitute a large fraction of the variance of the respective LF-ISOs of vorticity and divergence, it should not be surprising that both the barotropic vorticity and the baroclinic divergence LF-ISO have a northward propagating feature and are negatively correlated. Away from the equator, rainfall ISO and baroclinic divergence are in phase and lead the barotropic vorticity by 4-5 days. Whereas near the equator, the rainfall ISO and baroclinic divergence again peak roughly simultaneously and lag the barotropic vorticity by about 2-3 days. These lead lag relationships are important for developing a mechanistic understanding of the monsoon LF-ISO and its evolution from near-equatorial genesis to its dynamics and away from the equator.

The baroclinic nature of divergence can be attributed to the generation of surface low caused by convective heating with a single maximum in the mid-troposphere (Hazra & Krishnamurthy, 2015). This low results in the frictional convergence in the boundary layer, and to achieve the mass balance in the vertical column, this inflow is balance by upper lever divergence resulting in the baroclinic structure of divergence during an ISO event. As for the explanation of the barotropic nature of vorticity during ISO, further investigation is required, but a first-order scale analysis of the vorticity equation in the tropics does suggest that for large-scale flows, vorticity has a barotropic structure (Webster, 2020). Detailed analysis of the vorticity budget giving rise to this barotropic structure shall be undertaken in a subsequent study.

This study reveals the spatiotemporal structure of vorticity and divergence during low-frequency ISO in observations and brings out the similarities and differences between the two fields in the equatorial region and central Indian region. Coupled Earth System models are used to make projection of monsoon variability and change on various timescales. The findings of this study can be used to compare the fidelity of these state-of-the-art climate models in simulating these ISOs and the interaction between the associated variables. It is important to address whether the present generation of models obtain the structure of vorticity and divergence with reasonable accuracy during the monsoon intraseasonal phase. Additionally, a few simple idealized models have previously been developed to further mechanistic understanding of the processes giving rise to monsoon intraseasonal oscillations. Our present finding that vorticity is largely barotropic and that barotropic divergence is close to zero during these oscillations along with the fact that only few vertical modes are dominant during an ISO event is relevant for building a simple low-order model, containing only few modes, of monsoon intraseasonal oscillations. Such a model can help improve our understanding of the monsoon and its intraseasonal variability eventually leading to better long extended range forecast of the Indian summer monsoon.

Acknowledgement

The authors thank the European Centre for Medium-range Weather Forecast (ECMWF) and Tropical Rainfall Measuring Mission for providing ERA5 reanalysis products and the rainfall data respectively. The first author acknowledges Ministry of Human Resource Development for providing Prime Minister's Research Fellowship. We thank Vishal Dixit and J Srinivasan for their comments on an earlier draft of the manuscript.

References

Abhik, S., Halder, M., Mukhopadhyay, P., Jiang, X., & Goswami, B. N. (2013). A possible new mechanism for northward propagation of boreal summer intraseasonal oscillations based on TRMM and MERRA reanalysis. *Climate Dynamics*, *40*(7–8), 1611–1624. https://doi.org/10.1007/s00382-012-1425-x

Bellon, G., & Srinivasan, J. (2006). Comments on "Structures and mechanisms of the northward propagating boreal summer intraseasonal oscillation." *Journal of Climate*, *19*(18), 4738–4743. https://doi.org/10.1175/JCLI3861.1

DeMott, C. A., Stan, C., & Randall, D. A. (2013). Northward propagation mechanisms of the boreal summer intraseasonal oscillation in the ERA-interim and SP-CCSM. *Journal of Climate*, *26*(6), 1973–1992. https://doi.org/10.1175/JCLI-D-12-00191.1

Dixit, V., & Srinivasan, J. (2011). The role of vertical shear of the meridional winds in the northward propagation of ITCZ. *Geophysical Research Letters*, *38*(8), 1–5. https://doi.org/10.1029/2010GL046601

Drbohlav, H.-K. L., & Wang, B. (2005). Mechanism of the northward-propagating intraseasonal oscillation: Insights from a zonally symmetric model. *Journal of Climate*, *18*(7), 952–972.

Gadgil, S. (1995). Climate change and agriculture--an Indian perspective. *Current Science*, *69*(8), 649–659.

Ghil, M., Allen, M. R., Dettinger, M. D., Ide, K., Kondrashov, D., Mann, M. E., Robertson, A. W., Saunders, A., Tian, Y., Varadi, F., & Yiou, P. (2002). Advanced spectral methods for climatic time series. *Reviews of Geophysics*, *40*(1). https://doi.org/10.1029/2000RG000092

Goswami, B. N. (2005). South asian monsoon. In *Intraseasonal variability in the atmosphere-ocean climate system* (pp. 19–61). Springer.

Hazra, A., & Krishnamurthy, V. (2015). Space-time structure of diabatic heating in monsoon intraseasonal oscillation. *Journal of Climate*, *28*(6), 2234–2255. https://doi.org/10.1175/JCLI-D-14-00280.1

Hersbach, H., Bell, B., Berrisford, P., Hirahara, S., Horányi, A., Muñoz-Sabater, J., Nicolas, J., Peubey, C., Radu, R., Schepers, D., & others. (2020). The ERA5 global reanalysis. *Quarterly Journal of the Royal Meteorological Society*, *146*(730), 1999–2049.

Huffman, G. J., Bolvin, D. T., Nelkin, E. J., Wolff, D. B., Adler, R. F., Gu, G., Hong, Y., Bowman, K. P., & Stocker, E. F. (2007). The TRMM Multisatellite Precipitation Analysis (TMPA): Quasi-global, multiyear, combined-sensor precipitation estimates at fine scales. *Journal of Hydrometeorology*, *8*(1), 38–55.

Jiang, X., Li, T., & Wang, B. (2004). Structures and mechanisms of the northward propagating boreal summer intraseasonal oscillation. *Journal of Climate*, *17*(5), 1022–1039.

Karmakar, N., Chakraborty, A., & Nanjundiah, R. S. (2017). Space-time evolution of the low- and high-frequency intraseasonal modes of the Indian summer monsoon. *Monthly Weather Review*, *145*(2), 413–435. https://doi.org/10.1175/MWR-D-16-0075.1

Krishnamurthy, V., & Achuthavarier, D. (2012). Intraseasonal oscillations of the monsoon

circulation over South Asia. *Climate Dynamics*, *38*(11–12), 2335–2353. https://doi.org/10.1007/s00382-011-1153-7

Krishnamurthy, V., & Shukla, J. (2007). Intraseasonal and seasonally persisting patterns of indian monsoon rainfall. *Journal of Climate*, *20*(1), 3–20. https://doi.org/10.1175/JCLI3981.1

Li, B., Zhou, L., Qin, J., & Murtugudde, R. (2021). The Role of Vorticity Tilting in Northward-Propagating Monsoon Intraseasonal Oscillation. *Geophysical Research Letters*, *48*(13), 1–9. https://doi.org/10.1029/2021GL093304

Moron, V., Vautard, R., & Ghil, M. (1998). Trends, interdecadal and interannual oscillations in global sea-surface temperatures. *Climate Dynamics*, *14*(7–8), 545–569. https://doi.org/10.1007/s003820050241

Plaut, G., & Vautard, R. (1994). Spells of low-frequency oscillations and weather regimes in the Northern Hemisphere. In *Journal of the Atmospheric Sciences* (Vol. 51, Issue 2, pp. 210–236). https://doi.org/10.1175/1520-0469(1994)051<0210:SOLFOA>2.0.CO;2

Sikka, D. R., & Gadgil, S. (1980). On the maximum cloud zone and the ITCZ over Indian longitudes during the southwest monsoon. *Monthly Weather Review*, *108*(11), 1840–1853.

Webster, P. J. (2020). Dynamics of the Tropical Atmosphere and Oceans. In *Dynamics of the Tropical Atmosphere and Oceans*. John Wiley \& Sons.

Yang, Q., Khouider, B., Majda, A. J., & De La Chevrotière, M. (2019). Northward propagation, initiation, and termination of boreal summer intraseasonal oscillations in a zonally symmetric model. *Journal of the Atmospheric Sciences*, *76*(2), 639–668. https://doi.org/10.1175/JAS-D-18-0178.1

Yang, Y. M., Wang, B., & Lee, J. Y. (2019). Mechanisms of Northward Propagation of Boreal Summer Intraseasonal Oscillation Revealed by Climate Model Experiments. *Geophysical Research Letters*, *46*(6), 3417–3425. https://doi.org/10.1029/2018GL081612

Yasunari, T. (1979). Cloudiness Fluctuations Associated with the Northern Hemisphere Summer Monsoon. *Journal of the Meteorological Society of Japan. Ser. II*, *57*(3), 227–242. https://doi.org/10.2151/JMSJ1965.57.3_227

Yokoi, S., & Satomura, T. (2006). Mechanisms of the northward movement of submonthly scale vortices over the Bay of Bengal during the boreal summer. *Monthly Weather Review*, *134*(8), 2251–2265.

Zheng, B., & Huang, Y. (2019). Mechanisms of Northward-Propagating Intraseasonal Oscillation over the South China Sea during the Pre-Monsoon Period. *Journal of Climate*, *32*(11), 3297–3311. https://doi.org/10.1175/JCLI-D-18-0391.1